Mon. Not. R. Astron. Soc. **272**, 333–345 (1995)

First results from the UHRF: ultra-high-resolution observations of atomic interstellar lines towards ζ Ophiuchi

M. J. Barlow,[1] I. A. Crawford,[1,2] F. Diego,[1] M. Dryburgh,[1] A. C. Fish,[1] I. D. Howarth,[1] J. Spyromilio[2] and D. D. Walker[1]

[1] *Department of Physics and Astronomy, University College London, Gower Street, London WC1E 6BT*
[2] *Anglo-Australian Observatory, PO Box 296, Epping, New South Wales 2121, Australia*

Accepted 1994 August 15. Received 1994 August 11; in original form 1994 April 29

ABSTRACT

We present ultra-high-resolution observations of optical interstellar lines towards ζ Oph obtained during the commissioning phase of the new Ultra-High-Resolution Facility (UHRF) at the AAT. The UHRF has achieved its design resolving power of $R \approx 10^6$, and has very clearly resolved hyperfine splitting in three of the 11 identified Na I D-line velocity components towards ζ Oph. In addition, the *intrinsic* line profiles of the 3s–4p Na I doublet at 3302 Å have been measured for the first time. 12 velocity components are identified in the interstellar Ca II K-line absorption profile, of which seven have definite velocity counterparts in the Na I profile. Three of the Na I velocity components have *b*-values which correspond to a gas temperature of about 200 K, for the case of pure thermal broadening. The strongest component in the sightline (-14.8 km s^{-1}) was found to have a *b*-value of $0.6^{+0.2}_{-0.1}$ km s^{-1}, corresponding to a temperature of 500 K. If a true gas kinetic temperature of 54 K is assumed to apply to this component, from the H_2 rotational excitation temperature previously measured for the ζ Oph sightline, then the observed Na I and Fe I line profiles both imply an rms turbulent velocity of 0.4 km s^{-1} within the cloud, just less than the local sound speed. The observed Ca II linewidths are all significantly larger than those of the corresponding Na I components. The Ca II components are interpreted as arising from warm neutral material (intercloud medium) surrounding cooler clouds, while half of the Na I components arise from cool clouds and half arise from warm intercloud material. The measured Na I/Ca II column density ratios, and the inferred temperatures, are consistent with a model in which calcium is heavily depleted on to grains in cool clouds but is restored to the gas phase by impact desorption in the warm intercloud medium.

Key words: line: profiles – instrumentation: spectrographs – stars: individual: ζ Oph – ISM: atoms – ISM: clouds.

1 INTRODUCTION

The UCL Ultra-High-Resolution Facility (UHRF) is a significant new addition to the astronomical instrumentation available for optical studies of the interstellar medium. It was designed and built at University College London with the cooperation of the Anglo–Australian Observatory, and was commissioned at the coudé focus of the AAT in 1992 July. It is a quasi-Littrow echelle spectrograph, and is designed such that the diffraction-limited resolving power of the echelle grating is not significantly degraded by the other optical and detector elements. Specifically, the instrument is designed to achieve a maximum resolving power of $R \equiv \lambda/\Delta\lambda \approx 10^6$, corresponding to a velocity resolution of 0.3 km s^{-1} (FWHM). The UHRF was intended to be able to resolve absorption lines arising in the diffuse interstellar medium, even in the case where such lines are broadened only by thermal Doppler motions in gas with temperatures as low as 40 K. Most areas of spectroscopic astrophysical research have available to them instrumental resolving powers that are adequate to resolve fully the narrowest absorption or emission lines expected (see below). It is a remarkable fact that, until the advent of the UHRF, this situation had *never* been achieved in the field of interstellar absorption-line

spectroscopy. A full technical description of the spectrograph is given by Diego et al. (1995).

The velocity dispersion parameter of absorbing atoms, b, is related to the kinetic temperature of the gas, T_k, and the rms (Gaussian) turbulent velocity along the line of sight, v_t, through the expression

$$b = \left(\frac{2kT_k}{m} + 2v_t^2 \right)^{1/2}, \quad (1)$$

where k is Boltzmann's constant, and m is the mass of the atom or ion observed. The resulting FWHM of an unsaturated absorption line is $2b(\ln 2)^{1/2} = 1.665b$. From *Copernicus* observations of the rotational excitation of ultraviolet molecular hydrogen absorption lines in 60 sightlines, the typical diffuse cloud kinetic temperature has been estimated to be about 80 K (Savage et al. 1977), with excitation temperatures in the range 45–130 K being measured. For an element of atomic weight A and in the absence of turbulence, equation (1) becomes

$$b_A = 1.285\, A^{-1/2} (T_k/100\ \mathrm{K})^{1/2}\ \mathrm{km\ s^{-1}}. \quad (2)$$

The FWHM of an unsaturated Na I absorption line from a cloud with $T_k = 80$ K and no significant turbulent motions would therefore be 0.399 km s^{-1}, while an unsaturated K I absorption line would have a FWHM of 0.306 km s^{-1}. To match these intrinsic linewidths requires the use of resolving powers of $R = 7.5 \times 10^5$ for Na I, and $R = 9.8 \times 10^5$ for K I. The minimum cloud temperature that can be measured by an instrument scales inversely as the square of the resolving power – a resolving power of 5×10^5 corresponds to a temperature of 200 K for Na I, with temperatures about a factor of 2 smaller being measurable in spectra of high signal-to-noise ratio (S/N) by allowing for broadening by the instrumental profile (Hobbs & Welty 1991). A resolving power of one million corresponds to $T = 50$ K for Na I (before deconvolution), putting the UHRF squarely in the range needed to measure the temperatures of interstellar clouds.

The direct measurement of the b-values for species with significantly different atomic weights, for the *same* velocity component, can enable the derivation of both the kinetic temperature and the turbulent-velocity dispersion within the absorbing cloud. This provides a very direct, model-independent, and unambiguous method for deriving the temperatures of the various observable phases of the interstellar medium in a variety of sightlines. For example, when convolved with an instrumental FWHM of 0.30 km s^{-1}, an unsaturated Na I line from a cloud with $T_k = 80$ K and no turbulent motions would produce a FWHM of 0.499 km s^{-1}; an unsaturated K I 7699-Å line from the same cloud would yield a FWHM of 0.429 km s^{-1}; and the ^{7}Li I 6708-Å doublet lines would each have a FWHM of 0.783 km s^{-1}. The kinetic temperature and any turbulent motions within such a cloud could thus be determined using the UHRF.

1.1 The Ultra-High-Resolution Facility

The origins of the UHRF project to provide a permanent facility at the AAT for ultra-high-resolution spectroscopy are described by Diego et al. (1995). In its final form, the UHRF shares the east coudé room of the AAT with the UCL Echelle Spectrograph (UCLES, Walker & Diego 1984; Walker et al. 1986), but is effectively a separate spectrograph with its own 31.6 g mm^{-1} echelle, sharing only the pre-slit facilities and control software with UCLES. Order separation is provided by grating cross-dispersion. Additional resources were provided by the AAO in order to develop the UHRF as a fully common-user facility. In addition to its prime resolving power mode of one million, designed for interstellar absorption-line spectroscopy, the UHRF has lower resolution modes of 3×10^5 and 6×10^5, suitable for investigating a range of specialized stellar astrophysics topics.

1.2 Hyperfine-split Na lines

The transitions of the Na I D-line resonance doublet, at 5889.9512 and 5895.9243 Å (Morton 1991), are each split by the hyperfine interaction into two components, the D_2 subcomponents being separated by 1.01 km s^{-1}. The resolution of this hyperfine splitting requires cloud b-values less than 0.7 km s^{-1}, i.e., temperatures less than 700 K (see, e.g., Hobbs 1969b). Interstellar hyperfine components were first resolved by Wayte, Wynne-Jones & Blades (1978) in the Na I D-line spectrum of α Cyg, by using a Fourier transform spectrometer with a resolving power of 6×10^5. Similar hyperfine splitting was also observed in the Na I D-line spectrum of δ Cyg, with the same instrument (Blades, Wynne-Jones & Wayte 1980). Pettini (1988) used the Peter Gillingham Spectrograph (Gillingham 1988) to observe interstellar Na I D lines in the line of sight to SN 1987A and resolved Na D hyperfine splitting in a number of velocity components. Recently, Hobbs & Welty (1991) have observed the Na I D_1 line towards α and δ Cyg and four other stars, by using the McDonald Observatory 2.7-m telescope coudé echelle spectrograph in double-pass mode, with $R = 5 \times 10^5$. Each of the above studies that utilized resolving powers in excess of 5×10^5 found that virtually all unsaturated and unblended Na I velocity components exhibit hyperfine splitting, indicating very low turbulent velocities.

In addition to the Na I 3s–3p D-line resonance doublet at 5890, 5896 Å, the Na I 3s–4p UV ($\lambda\lambda$3302.368, 3302.978) doublet is also accessible from the ground, with each of the doublet transitions again split by the hyperfine interaction into two components, separated by 0.6 km s^{-1}. The f-values of the UV lines are 70 times smaller than for the D doublet (Morton 1991). Absorption components which are heavily saturated in the D lines can therefore have their intrinsic parameters accurately determined from observations of the Na I 3302-Å lines, so that observations with the UHRF can, in principle, allow the intrinsic linewidths and column densities to be accurately measured for *all* Na I velocity components along a line of sight.

Here we report observations of interstellar lines towards the bright southern star ζ Oph, which has a very well-studied interstellar sightline (Herbig 1968; Morton 1975; Savage, Cardelli & Sofia 1992). The observations were obtained during the UHRF commissioning phase in 1992 July, and during later runs in 1993 May (Na D), 1993 June (Fe I) and 1994 January (Ca II). These observations indicate that the instrument has successfully reached its intended resolving power, and provide important new information on the structure of the interstellar medium along this interstellar sightline.

2 OBSERVATIONS AND DATA REDUCTION

The interstellar lines observed are listed in Table 1. As these observations were obtained primarily to characterize the performance of the instrument during commissioning, they are somewhat inhomogeneous in nature.

A range of slit widths was used, as well as two confocal image slicers (Diego 1993) – the first, used in 1992 July, had 17 slices, each of width 35 μm and length 1 mm, while the second, used from 1993 May onwards, had 35 slices, each of width 30 μm and length 1 mm (at the *f*/37.5 coudé focus of the AAT the plate scale is 710 μm per arcsec). The resolving power corresponding to each spectrum, determined from the profile of an unresolved stabilized He–Ne laser line, as described in Section 2.3, is listed in Table 1. Table 1 also lists the dispersion (Å mm^{-1}), the spectral coverage of the detector (blue-coated Thomson CCD, 1024 × 1024 19-μm pixels, except for the Na I λ3302 spectrum, for which a blue-sensitive Tektronix CCD with 1024 × 1024 24-μm pixels was used), the exposure time for each spectral region, and the overall number of detected electrons above background that were obtained per collapsed CCD spectral channel. Most of the spectra reported here were obtained through variable amounts of cloud, so the numbers in Table 1 do not provide a useful guide to the instrumental throughput. A better indication of the throughput is provided by a Na I D_1 observation of the $V = 2.49$ star κ Vel, obtained in clear conditions on 1993 May 9, for which the 35-slice image slicer yielded 50 000 electrons above background per 19-μm spectral element in a 600-s exposure.

The spectra were extracted from the CCD images using the FIGARO data reduction package (Shortridge 1988) on the University College London STARLINK node. Owing to special circumstances, resulting in part from the fact that these observations were obtained during the commissioning of the spectrograph, three aspects of the calibration procedure deserve special comment.

2.1 Background removal

The detector backgrounds were found to be very high in the 1992 July commissioning-run spectra, and this has adversely affected the S/N ratios [compare the S/N ratio illustrated in fig. 11 of Diego et al. (1995) with the 6700 counts above background listed for it in Table 1]. These unusually high backgrounds were found to be principally due to scattered red stellar photons reaching the detector. The subsequent addition of more comprehensive baffling and the use of broad-band filtering for the UV spectral region have greatly reduced the observed background levels. For the spectra observed with a single-slit aperture, the backgrounds were determined from the interorder region and subtracted. In spite of the very high backgrounds, this correction appears to have worked well for most of the lines. For example, after background subtraction, the flat cores of the saturated Na D lines were found to have zero residual intensity; however, there is evidence (discussed in Section 3.4) that this procedure had not successfully corrected for all the scattered light at the wavelengths of the Na I 3s–4p doublet (3302 Å).

For the spectra obtained with an image slicer, the background calibration is complicated by the need to compress the very long output slit (10 mm in the case of the 17-slicer, and 20 mm for the 35-slicer) before it reaches the detector (20 mm is somewhat longer than the Thomson CCD, and without compression the read-out noise would be prohibitive). This was accomplished by means of a cylindrical lens placed immediately in front of the detector. Unfortunately, the presence of this lens meant that it was not possible to measure the interorder light directly (all light falling on to the lens, order and interorder, is focused on to a 1-mm wide strip running down the centre of the CCD). For lines that are known to be saturated (e.g., the Na D lines towards ζ Oph), the background can be obtained directly from the residual intensity within the flat line core (it amounted to approximately 5 per cent for the 1993 spectra listed in Table 1), but it could not be reliably determined for other lines observed using the cylindrical lens.

This inability to measure the interorder light directly while using a cylindrical lens with the image slicer was the major limiting factor in the scientific usefulness of the UHRF as configured prior to 1994 January. In an attempt to solve this problem, the cylindrical lens has since been eliminated and the 35-slicer masked: the resulting spectrum then fills about two-thirds of the area of the CCD (which is read out with four- or eight-pixel binning in the spatial direction), so

Table 1. Interstellar lines observed towards ζ Oph with the UHRF. *R* is the measured spectroscopic resolving power; $\Delta\lambda_{CCD}$ is the wavelength coverage of the 1024^2 Thomson CCD detector; the final column gives the overall number of detected electrons above background per collapsed 19-μm spectral element (except for the 1994 April Na UV spectrum, for which a 1024^2 Tektronix CCD with 24-μm pixels was used).

Line	U.T. Date	Slit	*R* (×10^5)	Disp. (Å mm^{-1})	$\Delta\lambda_{CCD}$ (Å)	Total Exp. (*n*×exp.)	Total Counts
Na I D_2	21-7-92	10 μm	9.9	0.13	2.6	2 × 1800s	6700
Na I D_2	10-5-93	35-slicer	9.4	0.13	2.6	1 × 1200s	31500
Na I D_1	10-5-93	35-slicer	9.4	0.13	2.6	2 × 1200s	65500
Na I λ3302	28-4-94	35-slicer*	9.4	0.072	1.8	2 × 1800s	2800
Ca II K	24-1-94	35-slicer*	9.4	0.086	1.7	1 × 2000s	3800
Fe I λ3719	04-6-93	35-slicer	9.4	0.089	1.7	2 × 1800s	31000

*Masked to 18 slices and cylindrical lens removed (see text, Section 2.1).

that the signal on either side of the stellar spectrum can be used to estimate the interorder background. This configuration was used for the 1994 Ca II and Na I λ3302 spectra reported here.

2.2 Wavelength calibration

Wavelength calibration was achieved by means of observations of a Th–Ar lamp. However, owing to the very high dispersion of the UHRF, only a restricted wavelength range (typically ~2 Å; cf. Table 1) falls on the detector at any one time. This is too small a wavelength coverage to guarantee that sufficient bright Th–Ar arc lines are available for wavelength calibration at each wavelength of interest.

Of the present observations, the Ca II K (3933.663-Å) spectral region was found to be the best provided for, with four Th–Ar lines identified within the 1.8-Å coverage of the detector. The expected near-perfect linearity of the dispersion over the small wavelength range that can be observed (together with the accuracy of the Th–Ar wavelengths tabulated by Palmer & Engelman 1983) is confirmed by the fact that a *linear* fit to these four lines resulted in an rms residual of 0.001 Å (corresponding to 0.08 km s^{-1}). Similarly, a linear fit to the positions of the 6328.160-Å laser line and two Th arc-lines occurring at the same setting gave a formal rms residual of 5×10^{-4} Å and a dispersion of 2.874×10^{-3} Å pixel^{-1}, corresponding to 0.1513 Å mm^{-1} (ray-tracing predicted a dispersion of 0.1521 Å mm^{-1} at this wavelength).

The accuracy found for the linear fit to the lines in the Ca K and laser-line spectral regions shows that the assumption of a linear pixel versus wavelength scale should not introduce significant errors into the wavelength calibration of other spectral regions. Insufficient known Th–Ar lines were found for the independent calibration of any of the four Na spectra. In the case of the UV lines, where both lines fit in the same frame, the corresponding emission lines from a small Na discharge lamp were used to provide a laboratory wavelength scale (again assuming linear dispersion over the 1.4-Å coverage of the detector).

In the case of the D_2 line observed in 1992, only one Th–Ar line was found to be present, and this was combined with a subsequent exposure of the D_2 emission line of the Na lamp to create a pseudo-arc for wavelength-calibration purposes. As this provided only two calibration lines, and as the Na D emission line in the lamp was found to be intrinsically broad, this calibration was clearly unsatisfactory. Subsequent experiments revealed that by placing the Th–Ar lamp directly in front of the image-slicer aperture, rather than in the UCLES calibration unit where it normally resides, the throughput can be greatly increased, leading to the detection of many more faint (and previously unidentified) Th–Ar lines. In the case of the 1993 Na D observations reported here, the wavelengths of several Th–Ar lines within the narrow D_1 and D_2 spectral regions were determined by fitting a third-order polynomial to six previously identified Th–Ar lines in the region 5885.7–5890.0 Å (Palmer & Engelman 1983; the rms residual to the fit was 3.5×10^{-4} Å). Fits to these newly identified lines within the Na D line spectral regions were found to give rms residuals of 6×10^{-4} Å (D_2) and 1×10^{-4} Å (D_1) (the lines are stronger in the latter case, hence the lower uncertainty to the fit). These correspond to residuals of 0.03 and 0.01 km s^{-1}, respectively.

In the Fe I spectral region, five Th–Ar lines were identified from the tabulation of Palmer & Engelman (1983); a linear fit resulted in an rms residual of 1.5×10^{-4} Å (0.01 km s^{-1}).

2.3 Instrumental resolution

As the UHRF easily resolves the Th–Ar arc lines, the instrumental resolution has been determined from the profile of a stabilized He–Ne laser located in the pre-slit calibration unit. The laser line at 6328.160 Å has an intrinsic linewidth ($\approx3\times10^{-5}$ Å) that is negligible compared to the instrumental response function. In 1992 July, it was determined that a 10-μm entrance slit yielded an instrumental FWHM of 0.302 ± 0.003 km s^{-1} ($R=993\,000\pm10\,000$). This laser profile is shown in Fig. 1(a). A 40-μm slit was found to give the slightly lower resolving power of $R=720\,000$ (Table 1).

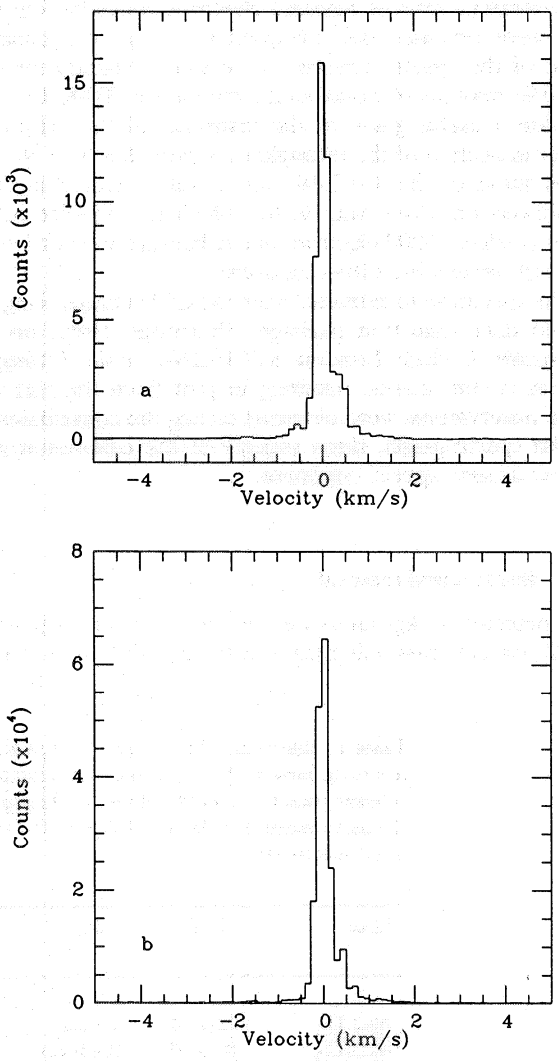

Figure 1. The UHRF instrumental response function, determined by means of a stabilized He–Ne laser, for (a) a 10-μm entrance slit (1992 July) and (b) the 35-slice image slicer (1993 May). The velocity scale is relative to the He λ6328.160 line, and Gaussian fits give FWHM of 0.302 ± 0.003 km s^{-1} ($R=9.93\times10^5$) and 0.320 ± 0.005 km s^{-1} ($R=9.38\times10^5$) for (a) and (b), respectively.

As implemented in 1992, the 17-slice image slicer was found to give a resolving power of $R = 660\,000$. In 1993, this slicer was replaced by a larger (35-slice) version, which was adjusted to produce a narrower slit, and thus a higher resolving power. Measurements made in 1993 May yielded an instrumental resolution of 0.320 ± 0.005 km s^{-1} ($R = 938\,000 \pm 15\,000$) with the new slicer. This profile is shown in Fig. 1(b). It will be apparent from Fig. 1 that the instrumental response is only just sampled properly by the detector. It would therefore be desirable to use the UHRF with a detector having a pixel size smaller than the 19-μm pixels of the Thomson CCD used here.

Strictly speaking, the calibration laser line profile only gives the instrumental resolution at the laser wavelength (6328.160 Å). However, from a consideration of the optical design of the spectrograph (based on ray-tracing models, Diego et al. 1995), we expect the resolution to be the same at all other wavelengths. We have confirmed this assumption by borrowing a stabilized green He–Ne laser from the Australian CSIRO National Measurement Laboratory and observing its line at 5433.647 Å. This yielded a FWHM of 0.318 ± 0.008 km s^{-1} ($R = 943\,000$), in excellent agreement with that derived from the red laser line and confirming the validity of the ray-tracing models. We note that most of the interstellar lines reported in this paper have been fully resolved (i.e. are much broader than the instrumental resolution), and that resolving powers in the range 700 000 to 940 000 have a negligible effect on the line-profile parameters derived in Section 3.

3 RESULTS

The spectra of ζ Oph are shown in Figs 2–6. The observed line profiles are plotted as histograms, where each bin corresponds to a single 19-μm CCD channel. Theoretical line profiles, discussed in the following sections, are plotted as smooth curves superimposed on the observed line profiles.

3.1 Fitting procedures

Theoretical absorption profiles were calculated with the interstellar-line modelling routines in the spectrum analysis program DIPSO (Howarth & Murray 1988). These routines were modified to allow for the full effects of hyperfine structure, and the necessary atomic data were taken from the recent compilation by Morton (1991). The essential assumption for the line-profile calculations is that each cloud can be modelled as a homogeneous, pure-absorption slab with a Gaussian line-of-sight velocity dispersion (as is appropriate for pure thermal broadening or if the turbulent velocities have a Gaussian distribution).

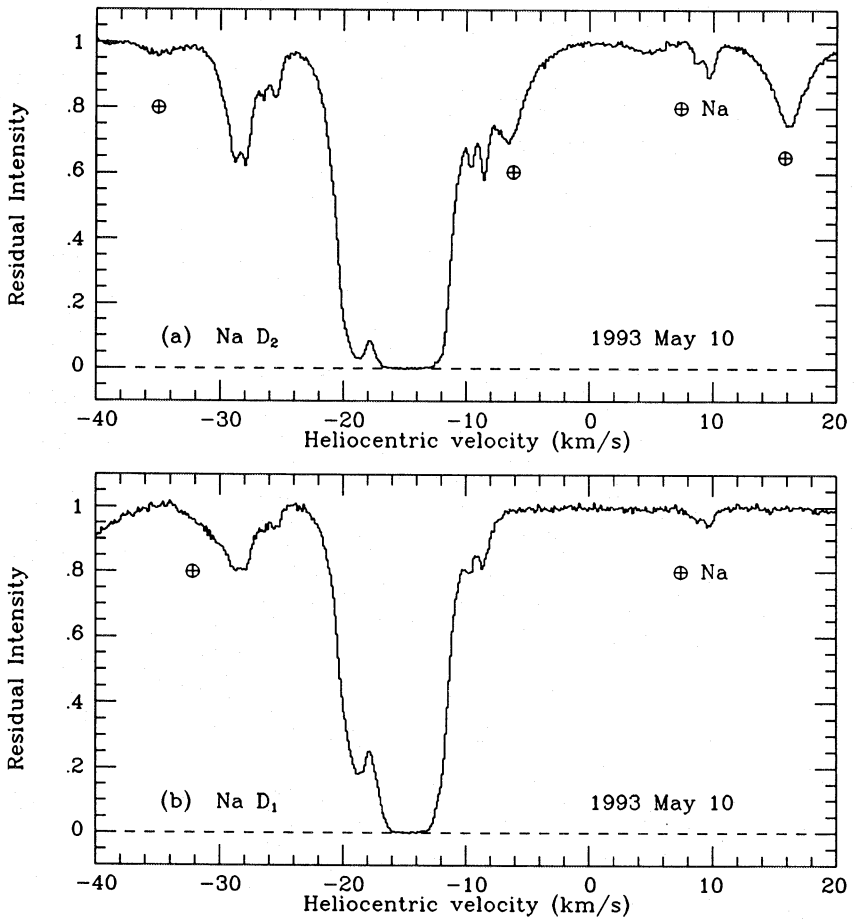

Figure 2. The interstellar Na D lines observed towards ζ Oph with the UHRF in 1993 May. The observed spectra are plotted as histograms, where each bin corresponds to a single 19-μm CCD column. Telluric absorption lines are indicated; note the clear detection of atmospheric Na absorption in the 1993 spectra.

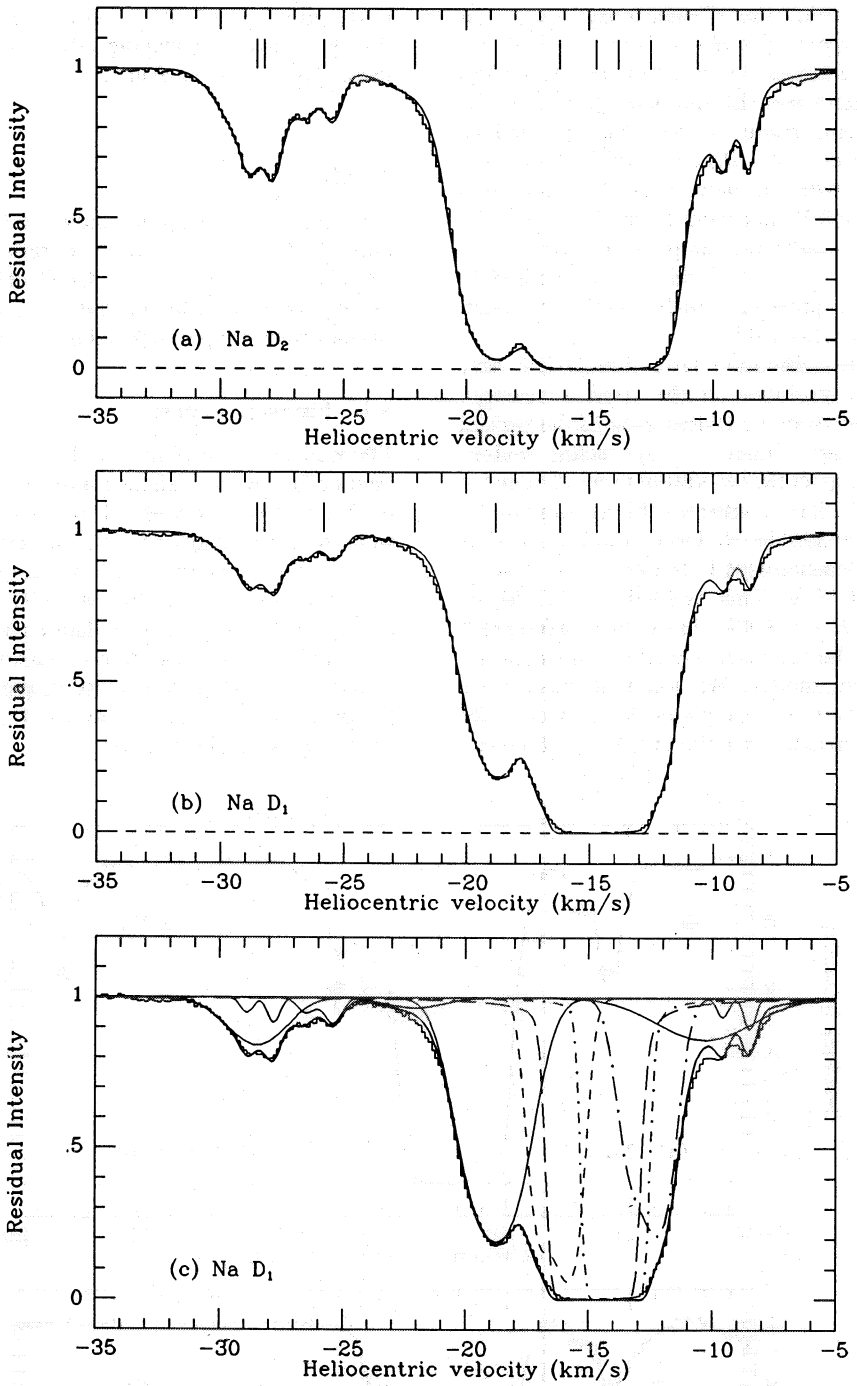

Figure 3. Theoretical line profiles compared with the observed profiles of the interstellar Na D lines towards ζ Oph. The line-profile parameters are given in Table 2, and the velocities of the 11 components in the fit are marked by vertical tick marks. In (c), we show the individual profiles of all the components present in the D_1 line.

The calculated line profiles were convolved with the appropriate instrumental response (Table 1) and compared with the observed line profiles. The free parameters (heliocentric velocity, velocity dispersion b, and column density N) were adjusted 'by hand' until a satisfactory fit was achieved. The parameters were then further adjusted to determine the extreme range of parameter values which gave tolerable fits. A single set of model parameters was adopted which gave an acceptable fit to all the Na lines, with a minimum number of velocity components. A separate model was constructed for the Ca K line. The best-fitting parameters and corresponding allowed ranges are summarized in Table 2.

3.2 The Na I D lines

The highest resolution spectrum obtained during the 1992 July commissioning run was of the sodium D_2 line (λ5889.951), for which two 1800-s exposures were obtained using a 10-μm entrance slit, giving a resolving power of

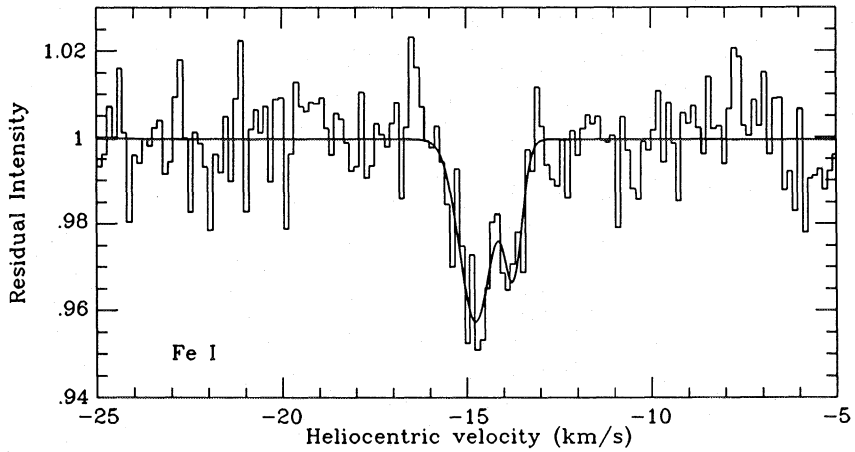

Figure 4. The Fe I line observed towards ζ Oph in 1993 June. Note the presence of two velocity components, separated by 1.02 ± 0.11 km s^{-1}.

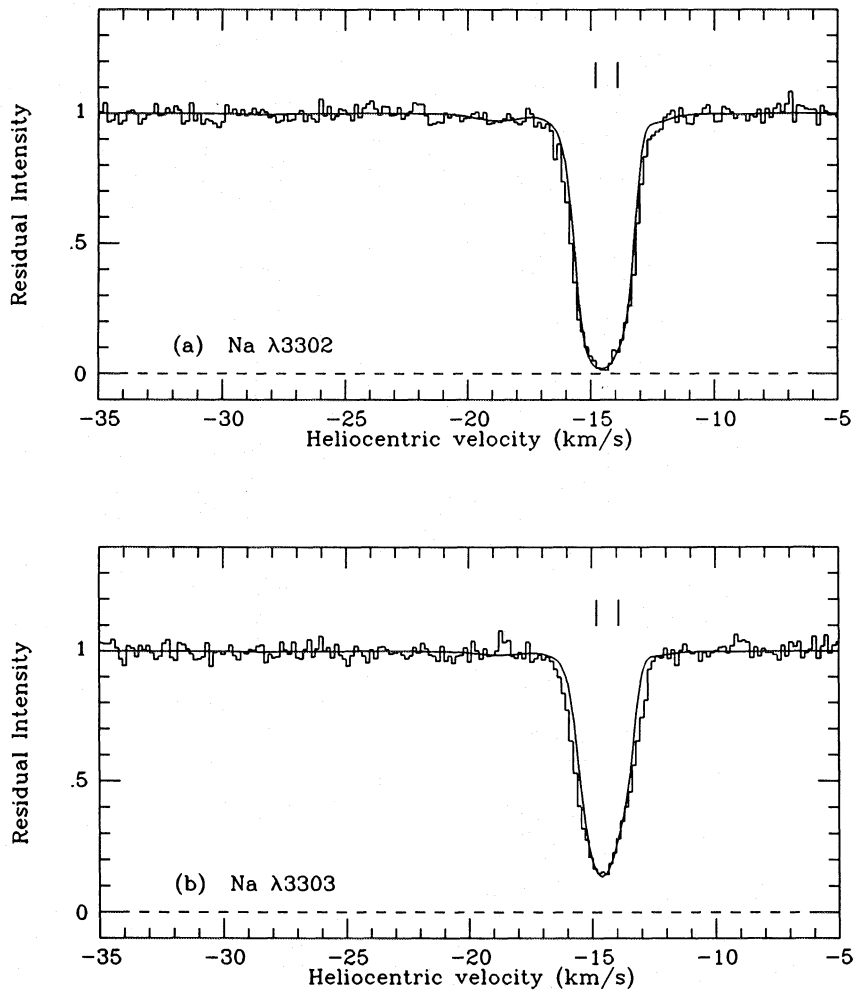

Figure 5. The interstellar Na UV doublet observed towards ζ Oph. The line-profile parameters for the model fit are given in Table 2. The velocities of the two components assumed to be present within the line are marked by vertical tick marks (see text for discussion).

990 000 (Table 1). This corresponds to a velocity resolution of 0.30 km s^{-1} (FWHM), and to our knowledge is the highest resolution optical stellar spectrum ever obtained. A plot of this spectrum (first shown in the 1992 July issue of the AAO Newsletter) is presented by Diego et al. (1995). In 1993 May, the 35-slice image slicer was used to obtain much higher S/N spectra of the D_2 and D_1 lines at a resolving power of 940 000. These are shown in Figs 2(a) and (b), respectively.

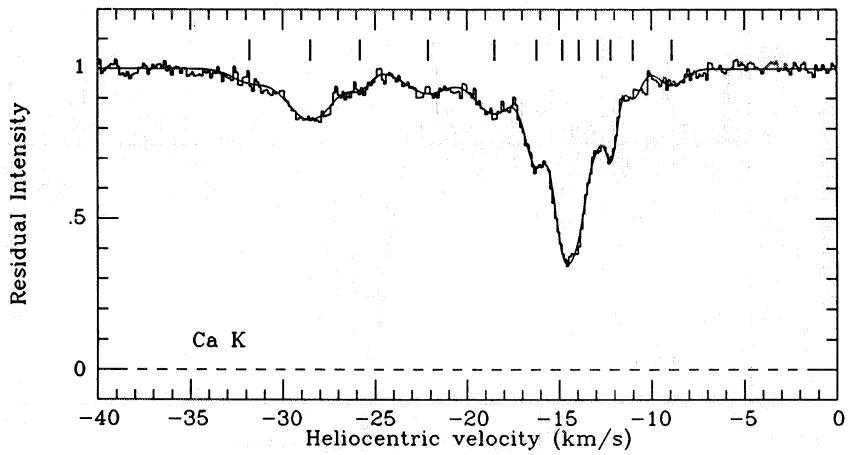

Figure 6. The interstellar Ca K line observed towards ζ Oph. The line-profile parameters for the model fit are given in Table 2, and the velocities of the 12 identified velocity components are indicated by vertical tick marks.

Table 2. Line-profile parameters for the Na I and Ca II lines observed towards ζ Oph with the UHRF. To obtain LSR velocities, add 13.7 km s^{-1} to the listed values of $v_{\rm helio}$.

Na D lines			Na λ3302 doublet			Ca K line		
$v_{\rm helio}$ (km s^{-1})	b (km s^{-1})	Log N (cm^{-2})	$v_{\rm helio}$ (km s^{-1})	b (km s^{-1})	Log N (cm^{-2})	$v_{\rm helio}$ (km s^{-1})	b (km s^{-1})	Log N (cm^{-2})
...	...	...	...	...	...	−31.8	$1.3^{+0.7}_{-0.3}$	$10.20^{+0.20}_{-0.10}$
−28.5	$1.4^{+0.1}_{-0.3}$	$11.00^{+0.05}_{-0.10}$	...	...	...	−28.5	$1.8^{+0.1}_{-0.2}$	$10.96^{+0.04}_{-0.06}$
−28.2	$0.35^{+0.07}_{-0.07}$	$10.30^{+0.10}_{-0.10}$	...	...	...	...	...	...
−25.8	$0.50^{+0.10}_{-0.10}$	$10.45^{+0.05}_{-0.15}$	...	...	...	−25.8	$0.8^{+0.2}_{-0.2}$	$10.10^{+0.25}_{-0.10}$
−22.1	$1.4^{+0.6}_{-0.4}$	$10.30^{+0.10}_{-0.20}$	...	...	...	−22.1	$1.7^{+0.3}_{-0.2}$	$10.60^{+0.15}_{-0.10}$
−18.8	$1.3^{+0.2}_{-0.2}$	$11.96^{+0.10}_{-0.10}$	...	...	...	−18.5	$1.5^{+0.3}_{-0.4}$	$10.82^{+0.08}_{-0.17}$
−16.2	$0.60^{+0.20}_{-0.20}$	$12.00^{+0.10}_{-0.10}$	...	...	...	−16.2	$0.80^{+0.15}_{-0.10}$	$10.92^{+0.13}_{-0.07}$
−14.7	0.60	13.80	−14.8	$0.60^{+0.20}_{-0.10}$	$13.80^{+0.10}_{-0.10}$	−14.8	$0.65^{+0.10}_{-0.15}$	$11.20^{+0.10}_{-0.15}$
−13.8	0.40	13.30	−13.9	$0.40^{+0.20}_{-0.20}$	$13.30^{+0.15}_{-0.20}$	−13.9	$0.65^{+0.05}_{-0.25}$	$11.05^{+0.15}_{-0.30}$
...	...	...	...	...	...	−12.9	$0.5^{+0.5}_{-0.2}$	$10.50^{+0.40}_{-0.20}$
−12.5	$0.75^{+0.30}_{-0.20}$	$11.80^{+0.20}_{-0.20}$	...	...	...	−12.2	$0.40^{+0.05}_{-0.20}$	$10.60^{+0.10}_{-0.40}$
−10.6	$2.0^{+0.5}_{-0.5}$	$11.00^{+0.15}_{-0.15}$	...	...	...	−11.0	$0.6^{+0.4}_{-0.1}$	$10.25^{+0.15}_{-0.20}$
−8.9	$0.35^{+0.10}_{-0.15}$	$10.50^{+0.10}_{-0.20}$	...	...	...	−8.9	$0.9^{+0.6}_{-0.2}$	$10.15^{+0.20}_{-0.15}$

Although the telluric H_2O absorption features were much stronger during the latter observations, the following analysis is based primarily on these spectra because of the much improved values of S/N.

In addition to several atmospheric water vapour lines, the spectra obtained of the Na D region in 1993 May also exhibit telluric Na absorption with the hyperfine structure clearly resolved (cf. Figs 2a and b). McNutt & Mack (1963) noted that telluric Na D absorption was only detectable during the northern winter; various Na D spectra that we have obtained with the UHRF have revealed telluric Na D absorption only during the southern winter.

It is apparent by inspection that at least five discrete velocity components are present in the Na D lines towards ζ Oph, as was first noted by Hobbs (1969a) in his pioneering high-resolution study ($R \approx (1\text{–}2) \times 10^5$; see Section 3.3) of interstellar line profiles. However, detailed line-profile modelling of the present data requires the presence of at least five additional components, and below we discuss the basis for our final model, which contains 11 components.

Table 2 gives the parameters which describe the absorption components identified in the D lines. Theoretical line profiles with these parameters are shown as smooth curves superimposed on the data in Figs 3(a) and (b). Fig. 3(c) shows the profiles of all 11 individual components which are included in the overall fit. The atmospheric water lines have been removed from the spectra shown in Fig. 3 by dividing by a telluric template spectrum obtained from UHRF observations of the nearby, unreddened star α Eri (a copy of this telluric template spectrum is available upon request); before division, the optical depths of telluric lines in the α Eri template spectrum are scaled to match those of unblended telluric lines in the target spectrum of interest. As the D_2 and D_1 lines are affected differently by the atmospheric water

lines (the former by a strong water line in the red wing, and the latter by a weaker line in the blue wing; cf. Fig. 2), this contamination has not seriously affected the derivation of the interstellar line profile parameters.

As already noted, in addition to the five absorption components which are obvious by inspection, a further six components are required to obtain a satisfactory model fit. The justification for these components is now given.

(i) The -28 km s^{-1} feature must contain two components. One of these has a moderately large b-value (to reproduce the width of the feature) and the second a rather small one (to allow the hyperfine structure to be resolved in the bottom of the line). The near-coincidence of the central wavelengths suggests that both components may be associated with the same interstellar complex (see Section 4).

(ii) The strong feature at -19 km s^{-1} has absorption in the blue wing which can only be reproduced by introducing an additional cloud component at ~ -22 km s^{-1}. A component at this velocity is clearly present in Ca II (Fig. 6 and Section 3.5).

(iii) Similarly, the dominant, saturated feature at about -14 km s^{-1} requires components in both wings to 'fill in' the profile. These components are also easily identifiable in the Ca II profile (Section 3.5). Moreover, while not directly visible in the Na D data, there is now unequivocal evidence that the 'main' (-14 km s^{-1}) component towards ζ Oph is in fact double, consisting of two components approximately 1 km s^{-1} apart. A study of CO $J=2$–1 and 1–0 emission at high spatial resolution toward ζ Oph, by Le Bourlot, Gérin & Pérault (1989), found two velocity components separated by 1.18 km s^{-1}, and Crawford et al. (1994) found two narrow CH velocity components, separated by 1.10 km s^{-1}, on the basis of UHRF observations. Lambert, Sheffer & Crane (1990) found two narrow CN velocity components, separated by 1.18 km s^{-1}, while Crawford et al. (1994) found a separation of 1.15 km s^{-1} for these CN components.

In order to check that the double structure observed in the molecular lines is also present in neutral atoms, we observed the Fe I line at 3719.934 Å in 1993 June (cf. Table 1). The spectrum is shown in Fig. 4, where it will be seen that the line is clearly double. A least-squares Gaussian fit gives heliocentric velocities of -14.75 ± 0.07 and -13.73 ± 0.08 km s^{-1}, respectively (the linewidths correspond to b-values of 0.58 ± 0.13 and 0.30 ± 0.08 km s^{-1}). Following these considerations, and given the extra information provided by the Na UV lines (discussed in Section 3.4), the main Na and Ca features were modelled with two velocity components. A separation of 0.9 km s^{-1} was found to be most consistent with obtaining satisfactory fits to both the Na D and UV lines, with an uncertainty of about ± 0.1 km s^{-1}. This may be compared with the velocity separation found for Fe I (1.02 ± 0.11 km s^{-1}). The Na b-values and columns for these narrow components are constrained by the physical requirement that the Na D and UV lines must be described by the same cloud model (see Section 3.4). Thus our final model for the dominant D-doublet feature contains four components: two strong, narrow velocity components, which are constrained by other lines (particularly Fe I and the Na UV doublet), and two weaker and broader velocity components, which are required to 'fill in' the shoulders of the feature (and which are also visible in Ca K; Section 3.5). The resulting fit is still far from perfect, and we suspect that additional clouds may be present.

(iv) Finally, like the -28.2 km s^{-1} cloud, the low-b, -8.9 km s^{-1} feature must sit on a broader, weak line.

The most important result to emerge from these very high-resolution spectra is the clear resolution of hyperfine splitting in the -8.9, -25.8 and -28.2 km s^{-1} components. The hyperfine splitting amounts to 1.01 and 1.08 km s^{-1} for the D_2 and D_1 lines, respectively (McNutt & Mack 1963), and the importance of observing this structure in interstellar spectra was first stressed by Hobbs (1969b). Because of the high resolution ($R \gtrsim 5 \times 10^5$) necessary to resolve it, hyperfine structure has so far only been observed for a small number of interstellar sightlines (see Section 1.2). It had not, to the best of our knowledge, been reported previously for any of the ζ Oph components.

The hyperfine splitting is best resolved in the -8.9 km s^{-1} component, which immediately indicates that this component arises in much colder and/or less turbulent gas than the others. The line-profile modelling summarized in Table 2 indicates that the best-fitting b-value of the -8.9 km s^{-1} component is 0.35 km s^{-1}, and that the *maximum* possible value is 0.45 km s^{-1} (the uncertainty is mostly due to blending with a broad component deduced to be present at -10.6 km s^{-1}). In the absence of turbulence, these b-values correspond to a kinetic temperature of 170^{+110}_{-115} K; any turbulent motions would imply *lower* temperatures. The fact that the hyperfine structure is only just resolved in the comparably narrow -28.2 km s^{-1} component is principally due to blending with a broader component at almost the same velocity (-28.5 km s^{-1}).

From *Copernicus* observations of H_2 in the ζ Oph sightline, Savage et al. (1977) derived an excitation temperature of 54 ± 7 K from the relative populations of the $J=0$ and $J=1$ rotational levels of the ground vibrational state of H_2 (energy separation = 170 K). This may be compared with the somewhat lower value of 30 ± 10 K obtained from measurements of C_2 rotational excitation by van Dishoeck & Black (1986).

The -13.9 and -14.8 km s^{-1} velocity components seen in Na I are likely to be responsible for almost all of the observed molecular gas, but the Na I b-values for these two components, 0.60 and 0.40 km s^{-1}, correspond to significantly higher temperatures (500 and 220 K) than those derived from the rotational excitation of H_2 and C_2. It therefore appears that there must be a turbulent broadening contribution to the observed Na I linewidths of these components. For the dominant Na I component, that at -14.8 km s^{-1}, the b-value derived from the Na I UV lines is $0.60^{+0.20}_{-0.10}$ km s^{-1}, while the b-value derived from the Fe I 3719.9-Å line is 0.58 ± 0.13 km s^{-1}. If one assumes that the temperature of this component is 54 K, from the measured H_2 excitation temperature, then from equation (1) an rms turbulent velocity within the cloud of $0.40^{+0.15}_{-0.08}$ km s^{-1} is implied by our Na I observations, in excellent agreement with the value of 0.40 ± 0.09 km s^{-1} obtained from the Fe I observations (these conclusions are not changed if the lower kinetic temperature of 30 K is adopted). For an atomic hydrogen gas at 54 K (assuming He/H = 0.1 by number) the sound speed is 0.59 km s^{-1} (falling to 0.44 km s^{-1} for a molecular gas). Thus, if the kinetic temperature is as high as

54 K in this component, the turbulence is just subsonic. However, we note that, if the temperature is actually as low as the 30 K implied by the C_2 data of van Dishoeck & Black (1986), then our results would permit marginally sonic turbulence in the -14.8 km s^{-1} component. If a kinetic temperature of 54 K is also applicable to the -13.9 km s^{-1} component, then its b-value of 0.40 ± 0.20 km s^{-1} corresponds to an rms turbulent velocity of $0.25^{+0.15}_{-0.22}$ km s^{-1} (or 0.26 ± 0.16 km s^{-1} for $T = 30$ K). Thus turbulence in the -13.9 km s^{-1} component is almost certainly subsonic (and may be barely present if the b-value is at the lower end of its empirically determined range and the temperature is as high as 54 K).

3.3 PEPSIOS results

The only previous observations of the Na I D lines towards ζ Oph with a claimed resolving power approaching ours were reported by Hobbs (1969a, his fig. 3), who used a PEPSIOS triple-etalon Fabry–Perot interferometer. Hobbs was unable to make a direct measurement of his resolving power, but estimated $R = 6 \times 10^5$ from consideration of the instrument characteristics. However, we note that, even if PEPSIOS did indeed return that resolving power, Hobbs's data were sampled only every 0.5 km s^{-1} so that, by the sampling theorem, his effective resolving power could not have exceeded $R = 3 \times 10^5$.

Since Hobbs's data on this and other stars represent the most extensive and important sample of high-resolution interstellar absorption-line observations made to date, we thought it of interest to estimate the true resolving power of those observations. To do this, we convolved our own observations with a cubed Airy function (the most generous assumption concerning the PSF of a triple-etalon Fabry–Perot system), then binned them at Hobbs's sampling rate, and compared them with his observations, which we digitized from his paper. On this basis we estimate that the FWHM of the PEPSIOS response function in Hobbs's work corresponded to a resolving power in the range $R = (1\text{–}2) \times 10^5$, incapable of resolving Na D hyperfine structure and 5–10 times smaller than the directly measured PSF of the UHRF.

3.4 The Na I UV lines

The 3s–4p Na I λ3302 doublet lines have oscillator strengths that are only 1.4 per cent of those of the corresponding D lines (Morton 1991). The intrinsically weaker nature of these lines makes them less subject to saturation than the D lines, and some previous workers have attempted to obtain Na I column densities from them under the assumption that these lines always lie on the linear part of the curve of growth. The very high resolution of the present data allows us to check this assumption, and to measure the b-values directly from the resolved line profiles.

The UV Na I doublet lines observed towards ζ Oph are shown in Figs 5(a) and (b). Unfortunately, there is some uncertainty in the placement of the zero intensity level of these spectra. A straight subtraction of the interorder background, which worked well for the fully saturated D lines, left the stronger (λ3302) UV line with a core residual intensity of 0.13. However, there are reasons for believing that the core of this line actually approaches much more closely to zero residual intensity. The λ3303 line is significantly less saturated than the λ3302 line, and we found that, for a simultaneous fit to both lines to be obtained, an additional fraction of the observed continuum level had to be subtracted. Following this argument, the spectra shown in Fig. 5 have been corrected for the inferred amount of additional scattered light (10 per cent of the continuum intensity). Even if this argument is not accepted, it can still be shown that this relatively large zero-level uncertainty results only in additional uncertainties of, respectively, 10 and 30 per cent in the b- and N-values listed in Table 2. The equivalent widths of the $\lambda\lambda$3302 and 3303 lines before the additional continuum level correction was made were measured to be 26.3 ± 0.6 and 20.8 ± 0.5 mÅ, respectively, while after the additional continuum correction the equivalent widths were measured to be 29.2 ± 0.6 and 23.1 ± 0.6 mÅ. Previous measurements of the equivalent widths of these lines have been summarized by Crawford (1992); our corrected values are consistent with those of Herbig (1968) and Crawford (1992), agreeing more closely with the former.

The observations of the UV lines make it possible to place much tighter limits on the b- and N-values for the two main velocity components than is possible using the D lines alone (see Section 3.2 above). Moreover, the requirement that the same model be consistent with both the Na D and UV line profiles was found to be very limiting, particularly of the maximum permitted b-values. The smooth curves shown in Fig. 5 are theoretical profiles corresponding to the parameters given in Table 2. Although this model was found to be able to fit both the Na D and UV lines reasonably well (allowing for a 0.1 km s^{-1} global velocity shift between the two, which is plausibly due to wavelength calibration uncertainties), careful inspection reveals that the model profile is actually somewhat narrower than the observed width of the weaker UV line (Fig. 5b). While it was determined that a much better fit could be obtained for the UV lines by increasing the separation of the two components to 1.1 km s^{-1}, and increasing the b-values to 0.7 and 0.5 km s^{-1} (for the same total column density), this was found to be quite inconsistent with the observed profile of the D_1 line (making the fully saturated core much broader than observed).

It may be that the difficulty in fitting the Na D and UV lines adequately with two components implies that a third must be present within the velocity range occupied by the fully saturated D lines. Indeed, a better fit to the UV lines, which provides just as good a fit to the D lines, may be obtained with three very narrow components with the following parameters (v, b, log N): (-15.4 km s^{-1}, 0.3 ± 0.1 km s^{-1}, 13.2 ± 0.2 cm^{-2}); (-14.6 km s^{-1}, 0.5 ± 0.2 km s^{-1}, 13.7 ± 0.1 cm^{-2}); (-13.7 km s^{-1}, 0.3 ± 0.1 km s^{-1}, $13.2^{+0.1}_{-0.4}$ cm^{-2}). However, as there is no independent evidence for an additional component within this velocity range, our preferred model remains the two-component fit listed in Table 2. The main point to note is that, with two components, the b-values are constrained to be about 0.6 and 0.4 km s^{-1}, respectively. An additional component would force all three to be significantly narrower. To our knowledge, this is the first time that useful limits have been placed on the b-values of the Na UV lines towards ζ Oph.

3.5 The Ca II K line

The Ca II K-line spectrum was obtained in 1994 January with the use of a 35-slice image slicer, masked down to 18 slices so as to permit measurement of the interorder background (Section 2.1). The spectrum is shown in Fig. 6.

10 discrete velocity components are readily apparent in Fig. 6, and a further component (at -12.9 km s^{-1}) is inferred to be present from the line profile analysis. In addition, the main ('-14' km s^{-1}) feature has been fitted with two components, following the arguments presented in Section 3.2 (iii). Thus our final Ca K model contains a total of 12 discrete velocity components, most of which agree with those found in Na I (Table 2). We stress that all these components have been fully resolved (i.e. all have b-values much broader than the instrumental resolution).

The fact that the main component is unsaturated means that the Ca II spectrum reveals velocity structure on either side of it, which is masked in the D lines and undetected in the weak Na UV lines. In particular, narrow components are clearly present at -16.2 and -12.2 km s^{-1}, and clouds at these velocities were included in the modelling of the D lines (where their presence greatly eased the problem of fitting *both* D lines with the same model profile).

Finally, we note that additional velocity components may also be present; in particular, the relatively broad ($b = 1.8$ km s^{-1}) component at -28.5 km s^{-1} may mask a weak component corresponding to that at -28.2 km s^{-1} in Na I.

4 DISCUSSION

A current standard model of the thermal and density structure of the interstellar medium is due to McKee & Ostriker (1977). According to this model, a cold neutral medium (CNM), with a small volume filling fraction but containing most of the mass (cloud densities $n \sim 10$–1000 cm^{-3} and cloud temperatures $T_k \sim 30$–100 K), coexists in approximate pressure equilibrium with a hot ionized medium (HIM), with $n \sim 10^{-3}$ cm^{-3} and $T_k \sim 10^6$ K and a volume filling factor of $f \sim 0.7$, produced by the overlap of successive supernova remnants. According to the model, two further components should be found as coronae around the cold neutral medium: a warm ionized medium (WIM) and a warm neutral medium (WNM), each with $T_k \sim 8000$ K and $n \sim 0.15$ cm^{-3}, with the outer WIM having an ionization fraction ~ 0.7, produced by photoionization by hot OB stars, while the inner WNM around the cold phase is nearly neutral, with an ionization fraction ~ 0.1 maintained by X-rays penetrating from the HIM. This three-phase model of the ISM (cold, warm and hot) still appears viable, although Slavin & Cox (1993) have emphasized the degree to which the assumption of a large filling factor for the hot ionized medium depends on uncertainties in supernova rates and other parameters, and have shown that an intercloud medium whose volume is dominated by warm gas ($T_k \sim 8000$ K and $n \sim 0.15$ cm^{-3}) may be just as likely.

Of the 11 different Na I velocity components that we have identified (Section 3.2 and Fig. 3c), seven have radial velocities that match those of a Ca II velocity component to better than 0.3 km s^{-1} (Table 2; a further three Na I components have radial velocities that differ from those of a Ca II component by 0.3–0.4 km s^{-1}). For these seven velocity components, it is of interest to compare the widths of the respective sodium and calcium lines.

In the absence of turbulent broadening, equation (2) implies that, for the case of Na I, the kinetic temperature of an absorbing component is given by $T_k = 1393\,b^2$, while, for the case of Ca II, $T_k = 2422\,b^2$. Of the seven matched velocity components, the b-value of the Ca II component is found always to exceed that of the corresponding Na I component, by factors that range from 1.6 to 3.4 (i.e. by factors of 2.6 to 11.5 in temperature, if the broadening is purely thermal). Although the individual differences are significant at, typically, only the 1–2σ level, the probability that all seven Ca b-values should exceed the Na values by this amount is negligibly small. The possibility of systematic, wavelength-dependent errors in the adopted instrumental point spread function can also be discounted.

Although these sodium and calcium absorption components are at indistinguishable radial velocities, the systematic difference in linewidths implies that these features cannot arise from coextensive material. If turbulent broadening dominated, it would yield the same linewidth for all species; while absorption by coextensive material in which thermal broadening dominated would yield calcium linewidths *smaller* (by a factor of 1.3) than those of sodium.

On the basis of the linewidths reported in Table 2, we interpret the sodium components as arising (a) from cool clouds, corresponding to the cold neutral medium (e.g., the -28.2, -25.8, -16.2, -14.7, -13.8 and -8.9 km s^{-1} components), and (b) from warmer gas situated in transition regions around the cool clouds, corresponding to the warm neutral medium (e.g., the -28.5, -22.1, -18.8, -12.5 and -10.6 km s^{-1} components). On the other hand, the seven calcium components with the same radial velocities as the sodium components appear to arise only from the warm neutral medium. Amongst these seven velocity components, the -28.5 and -22.1 km s^{-1} components have the highest sodium and calcium b-values, corresponding to $T_k = 2730$ K for each of the sodium components and to $T_k = 7850$ and 7000 K for the respective calcium components, for the case of pure thermal broadening. These two velocity components also have the highest derived values for their calcium to sodium ratios; the ratio of Ca II to Na I column densities is 0.9 for the -28.5 km s^{-1} component and 2.0 for the -22.1 km s^{-1} component, compared to column density ratios of 0.4 to 0.002 for the five velocity components with lower b-values. We interpret this pattern as having two contributing causes. The first and probably lesser effect may be that sodium (I.P. = 5.1 eV) has a larger fraction in the form of unobservable Na II in warm regions ($T_k \geq 1000$ K) than in cool absorbing regions. The other factor is the effect of dynamic depletion (in cool regions) and desorption (in warm regions) on gas-phase abundances, particularly those of calcium (Barlow & Silk 1977; Barlow 1978). Due to the higher adsorption energy of calcium on grain surfaces (Barlow 1978), calcium atoms should be depleted from the gas phase relative to sodium atoms on a relatively rapid time-scale in the interiors of cool, high-density regions. [This time-scale is $\sim 3 \times 10^7 (50\,\mathrm{cm}^{-3}/n)(100\,\mathrm{K}/T_k)^{1/2}$ yr for calcium atoms in a cloud with hydrogen nucleon density n, temperature T_k and a dust-to-gas ratio corresponding to the model of Mathis, Rumpl & Nordsieck 1977.] Low gas-phase calcium-to-sodium ratios should therefore be exhibited by such cloud

regions. In higher temperature regions, chemisorbed particles on grain surfaces can be desorbed by impacting gas-phase atoms. From appendix A of Barlow (1978), it can be shown that calcium atoms adsorbed on either graphite or amorphous carbon, with an absorption energy of ~3.4 eV, will be desorbed from the surface in about 1000 yr when situated in a medium with $n = 0.1$ cm^{-3} and $T_k = 5000$ K. Warm intercloud regions should therefore exhibit a smaller degree of calcium depletion (the residual depletion being due to the calcium fraction locked up in refractory grains) and much higher gas-phase calcium-to-sodium ratios should be exhibited by such intercloud regions.

We attribute the fact that, for all seven matched velocity components, the calcium component is always broader than the sodium component to the existence of continuous temperature gradients across the warm neutral material, from the coolest regions at the boundaries with inner cold clouds to the warmest material at the boundaries with the ionized medium. Since the depletion of calcium will be least in the warmest gas, the warmest regions will dominate the Ca II absorption. On the other hand, since sodium is not expected to undergo significant gas-phase depletion or subsequent desorption, it will not be weighted to the highest temperature parts of the warm neutral medium – the abundance of Na I may, if anything, decrease in the hottest regions, due to an increased Na II fraction there. The narrow −28.2 km s^{-1} Na I absorption component (with $T_k = 170$ K, if thermally broadened) sits upon the broader −28.5 km s^{-1} component (with $T_k = 2730$ K for Na I and $T_k = 7850$ K for Ca II). It is tempting to associate the broad −28.5 km s^{-1} component with a warm neutral transition region that surrounds the −28.2 km s^{-1} cool cloud. The absence of a Ca II counterpart to the −28.2 km s^{-1} cool Na I component can be attributed to the high degree of calcium depletion expected in such a cloud.

5 CONCLUSIONS

The UHRF has achieved its design specification and has been demonstrated to be capable of yielding unique data. The main results to emerge from these commissioning observations are as follows.

(1) A total of 13 discrete Na I and Ca II velocity components have been deduced to exist in the line of sight to ζ Oph, significantly more than the number determined from lower resolution studies. Moreover, with the possible exception of the two narrowest Na D components, all of these have been fully resolved (i.e., they are shown to be broader than the instrumental resolution), and this has made it possible to determine very accurate *b*-and *N*-values (Table 2).

(2) Hyperfine structure has been resolved in Na D-line velocity components towards ζ Oph for the first time. In the case of the −8.9 km s^{-1} component, this observation enables us to obtain a best-fitting cloud-kinetic temperature of 170^{+110}_{-115} K, for the case of pure thermal broadening.

(3) The line profiles of the 3s–4p λ3302 doublet of Na I have been resolved for the first time. These profiles have resulted in the determination that $b = 0.60^{+0.20}_{-0.10}$ and $0.40^{+0.20}_{-0.20}$ km s^{-1} for the two strongest Na I components present towards ζ Oph, in reasonable agreement with values determined from the (comparably massive) CN molecule (Lambert et al. 1990; Crawford et al. 1994). If the H_2 rotational temperature of 54 K that has been measured for the ζ Oph sightline is adopted as the true kinetic temperature of the dominant Na I component (at −14.8 km s^{-1}), an rms turbulent velocity of 0.4 km s^{-1} is implied by both the Na I and Fe I line profiles, which is only just below the local sound speed for a predominantly molecular hydrogen gas.

(4) Seven of the 11 Na I velocity components have radial velocities that match those of a Ca II velocity component. In each case the *b*-value of the Ca II component is significantly larger than that of the corresponding Na I component. We intepret all of the observed Ca II components as arising from the warm neutral medium (intercloud medium) surrounding cold clouds. About half of the Na I components also originate from this warm medium, with the remainder originating from cold clouds. The implied temperatures, as well as the observed Na I to Ca II column density ratios, are consistent with a model whereby the depletion of sodium on to grains is relatively constant, whereas the gas-phase depletion of calcium is very large in cold regions, due to adsorption on to grains, but much less in warm regions, due to the desorption of calcium from grain surfaces by the more energetic ambient gas.

ACKNOWLEDGMENTS

We thank the SERC for funding the UHRF project, and we are grateful to the Director, Dr Russell Cannon, and the staff of the Anglo-Australian Observatory for their strong support and encouragement throughout the project. IAC thanks the SERC for PDRA support, and the Royal Society for the award of an Exchange Fellowship.

REFERENCES

Barlow M. J., 1978, MNRAS, 183, 417
Barlow M. J., Silk J., 1977, ApJ, 211, L83
Blades J. C., Wynne-Jones I., Wayte R. C., 1980, MNRAS, 193, 849
Crawford I. A., 1992, MNRAS, 259, 47
Crawford I. A., Barlow M. J., Diego F., Spyromilio J., 1994, MNRAS, 266, 903
Diego F., 1993, Appl. Opt., 32, 6284
Diego F. et al., 1995, MNRAS, 272, 323 (this issue)
Gillingham P. R., 1988, in Robinson L. B., ed., Instrumentation for Ground-Based Optical Astronomy; Present and Future. Springer-Verlag, New York, p. 134
Herbig G. H., 1968, Z. Astrophys., 68, 243
Hobbs L. M., 1969a, ApJ, 157, 135
Hobbs L. M., 1969b, ApJ, 157, 165
Hobbs L. M., Welty D. E., 1991, ApJ, 368, 426
Howarth I. D., Murray J., 1988, Starlink User Note No. 50
Lambert D. L., Sheffer Y., Crane P., 1990, ApJ, 359, L19
Le Bourlot J., Gérin M., Pérault M., 1989, A&A, 219, 279
McKee C. F., Ostriker J. P., 1977, ApJ, 218, 148
McNutt D. P., Mack J. E., 1963, J. Geophys. Res., 68, 3419
Mathis J. S., Rumpl W., Nordsieck K. H., 1977, ApJ, 217, 425
Morton D. C., 1975, ApJ, 197, 85
Morton D. C., 1991, ApJS, 77, 119
Palmer B. A., Engelman R., 1983, Atlas of the Thorium Spectrum. Los Alamos Natl. Lab. Rep. LA-9615
Pettini M., 1988, Proc. Astron. Soc. Aust., 7, 527

Savage B. D., Bohlin R. C., Drake J. F., Budich W., 1977, ApJ, 216, 291
Savage B. D., Cardelli J. A., Sofia U. J., 1992, ApJ, 401, 706
Shortridge K., 1988, Starlink User Note No. 86
Slavin J. D., Cox D. P., 1993, ApJ, 417, 187
van Dishoeck E. F., Black J. H., 1986, ApJ, 307, 332
Walker D. D., Diego F., 1985, MNRAS, 217, 355
Walker D. D., Diego F., Charalambous A., Hirst C. J., Fish A. C., 1986, Proc. SPIE 627. Int. Soc. Opt. Eng., Bellingham, p. 291
Wayte R. C., Wynne-Jones I., Blades J. C., 1978, MNRAS, 182, 5P